Applied Nanoscience (2021) 11:21–27
https://doi.org/10.1007/s13204-020-01582-w

ORIGINAL ARTICLE

Influence of chitosan modification on self-assembly behavior of Fe_3O_4 nanoparticles

Dongmei Zhang[1] · Xudong Zuo[2] · Peng Wang[3] · Wei Gao[4] · Lujun Pan[1]

Received: 30 March 2020 / Accepted: 12 October 2020 / Published online: 24 October 2020
© King Abdulaziz City for Science and Technology 2020

Abstract

Self-assembled Fe_3O_4 nanoparticles are attracting more and more interests in biomedical field, such as dual photoacoustic devices and magnetic resonance imaging. At present, however, the preparation of self-assembled Fe_3O_4 nanoparticles mainly relies on the modifications of some toxic polymers, such as 4-vinylpyridine, polyacrylonitrile, and phenol formaldehyde resin. Additionally, the synthetic methods used were too complicated. The biological toxicity and complex methods significantly limit the biomedical applications of self-assembled Fe_3O_4 nanoparticles. In this work, natural polysaccharide chitosan was used to modify Fe_3O_4 nanoparticles. The self-assembled Fe_3O_4 nanochains were obtained easily by controlling the ratio of chitosan and Fe_3O_4 nanoparticles. The formation mechanism of Fe_3O_4 nanochains was proposed and demonstrated by experiments and numerical simulation. It is found that the thickness of chitosan is a key factor that affects the magnetic field distributions and magnetic attraction of Fe_3O_4 nanoparticles. The prepared chitosan-modified Fe_3O_4 nanochains would be a promising candidate with good biocompatibility for biomedical applications.

Keywords Fe_3O_4 nanoparticle · Chitosan · Self-assembly · Magnetic materials

Introduction

In the past decade, self-assembly has emerged as a very attractive method for constructing ordered nanostructures, due to its scalability and simplicity (Lin et al. 2016; Berrod et al. 2015). Magnetic nanoparticles, which have unique properties for many applications especially in biomedical areas (Zou et al. 2018; Vergaro et al. 2011; Parekh et al. 2018; Lvov et al. 2011; Gao et al. 2020), are excellent building blocks for self-assembly (Li et al. 2018).

Magnetite (Fe_3O_4), as one of the most important magnetic materials with promising applications in numerous field (Wan et al. 2007; Wang et al. 2007), has received considerable attention in the study of self-assembled magnetic nanoparticles (Gong et al. 2010). With the efforts of many researchers, self-assembled Fe_3O_4 nanochains with various lengths and different shapes have been reported (Gong et al. 2010; Zhang et al. 2009; Kim et al. 2014). Song et al. designed a new model of vesicles assembled by "Janus" Au–Fe_3O_4 nanoparticles grafted with different hydrophilicity polymer on Au and Fe_3O_4 surfaces separately, and used the vesicles for dual photoacoustic and magnetic resonance imaging in vivo (Song et al. 2017). Although constructing various self-assembled Fe_3O_4 nanostructures has achieved

✉ Lujun Pan
lpan@dlut.edu.cn

Dongmei Zhang
zhangdm08@163.com

Xudong Zuo
zxdong@mail.dlut.edu.cn

Peng Wang
WP15242630598@yeah.net

Wei Gao
w.gao@auckland.ac.nz

1 School of Physics, Dalian University of Technology, Dalian 116024, People's Republic of China

2 School of Mathematics and Physics, Jiangsu University of Technology, Changzhou 213100, People's Republic of China

3 Physics Department, Xinzhou Teachers University, Xinzhou 034000, People's Republic of China

4 Department of Chemical and Materials Engineering, The University of Auckland, Auckland 1142, New Zealand

great success (Zhang et al. 2007), the methods applied are complicated and the polymers used are mostly toxic. Therefore, developing a facile method with nontoxic polymer for constructing self-assembled Fe_3O_4 nanostructures is still highly desired.

Chitosan, which is an abundant biopolymer extracted from crab and shrimp shells (Gortari and Hours 2013; Kandra et al. 2012), has attracted particular attention in a wide variety of fields because it is biocompatible, biodegradable, antimicrobial, environment friendly, and low cost (Silva et al. 2017; Sun et al. 2017; Verlee et al. 2017). Moreover, chitosan has a special characteristic of pH-sensitivity (Solubility decreases with increasing pH value), which may provide a new strategy to synthesize chitosan complex by adjusting the pH value.

Inspired by these promises, we have developed an efficient dissolution–precipitation route for the large-scale synthesis of self-assembled chitosan-modified Fe_3O_4 nanochains, which is different from the previous reports. The microstructure and magnetic properties of the as-synthesized Fe_3O_4 nanochains have been studied. Moreover, the formation mechanism of Fe_3O_4 nanochains have been proposed and demonstrated. The as-synthesized chitosan-modified Fe_3O_4 nanochains may be a promising candidate in biomedical applications, such as bio self-healing (Seifan et al. 2018), nucleic acid extraction (Oster et al. 2001), DNA detection (Wang et al. 2001) and protein–protein interaction (Schotte et al. 2012).

Materials and methods

Synthesis of Fe_3O_4 nanoparticles

0.4 g iron (III) chloride anhydrous ($FeCl_3$, Sinopharm Chemical Reagent Co., China), 3.2 g sodium acetate anhydrous (CH_3COONa, Tianjin Kermel Chemical Reagent Co., China) and 0.8 g polyethylene glycol 1000 (PEG, Sinopharm Chemical Reagent Co., China) were dispersed in 35 mL ethylene glycol ($(CH_2OH)_2$, Sinopharm Chemical Reagent Co., China) with stirring magnetically for 30 min. Then, the mixed solution were transferred into a 50 mL Teflon autoclave, heated to 180 °C and maintained for 16 h. After cooling to room temperature, the products were taken out and washed by ethanol and distilled water for several times.

Modification of chitosan

25 mg chitosan was dissolved in 17.25 mL distilled water with the presence of 250 μL acetic acid (CH_3COOH, Tianjin Kermel Chemical Reagent Co., China). 250 mg as-prepared Fe_3O_4 nanoparticles were dispersed in the mixed solution with stirring magnetically for 30 min. 1 mL ammonia solution (NH_4OH, Tianjin Kermel Chemical Reagent Co., China) was then added. After vigorous stirring for 24 h, the products were washed by ethanol and distilled water for several times and dried at 60 °C for 6 h. For comparison, Fe_3O_4 nanoparticles without chitosan modification and Fe_3O_4 nanoparticles modified with 75 mg chitosan were also prepared by the same method. We labeled the Fe_3O_4 nanoparticles without chitosan modification, Fe_3O_4 nanoparticles modified with chitosan of 25 mg and 75 mg as Fe_3O_4-1, Fe_3O_4-2 and Fe_3O_4-3, respectively.

Characterization

The morphology of the as-synthesized nanoparticles was characterized by scanning electron microscopy (SEM, FEI, QUANTA 450) and transmission electron microscopy (TEM, FEI, Tecnai F30). The crystal structure of nanoparticles was investigated by X-ray diffraction (XRD, Empyrean with Cu-Kα radiation). Magnetic properties were studied by vibrating sample magnetometry (VSM, LDJ Electronics Inc., Model 9600). The chitosan content was investigated by Fourier transform infrared spectrophotometer (FTIR, Bruker, EQUINOX55) and thermogravimetric analysis (TGA, Perkin Elmer Instruments model, STA 6000).

Results and discussion

The morphology of pristine Fe_3O_4 nanoparticles and chitosan-modified Fe_3O_4 nanoparticles are characterized by SEM and TEM images. It is observed from Fig. 1a that the pristine Fe_3O_4 nanoparticles agglomerate together disorderly due to their high surface energy and magnetic attraction. After the modification of chitosan (Fig. 1b), Fe_3O_4 nanoparticles are assembled to nanochains with several micrometers in length.

Figure 1c shows the typical TEM image of pristine Fe_3O_4 nanoparticles with sizes ranging from 100 to 300 nm. The HRTEM image in Fig. 1e shows the lattice parameter of 0.256 nm is consistent with the (311) plane in spinel magnetite. Figure 1d, f are TEM images of the chitosan-modified Fe_3O_4 nanoparticles. After adding chitosan, a uniform coating on an entire nanoparticle surface with an average thickness of 10.8 nm is formed. Figure 1g, h are the selected area electron diffraction patterns of a pristine Fe_3O_4 nanoparticle and a chitosan-modified Fe_3O_4 nanoparticle, respectively. Five obvious diffraction rings match well with standard spinel Fe_3O_4 diffraction pattern.

XRD has been used to investigate the crystal structure of nanoparticles, and the obtained XRD patterns are shown in Fig. 2. All peaks can be indexed to the standard spinel structure (JCPDS No. 01-1111), and no peaks from impurities are found.

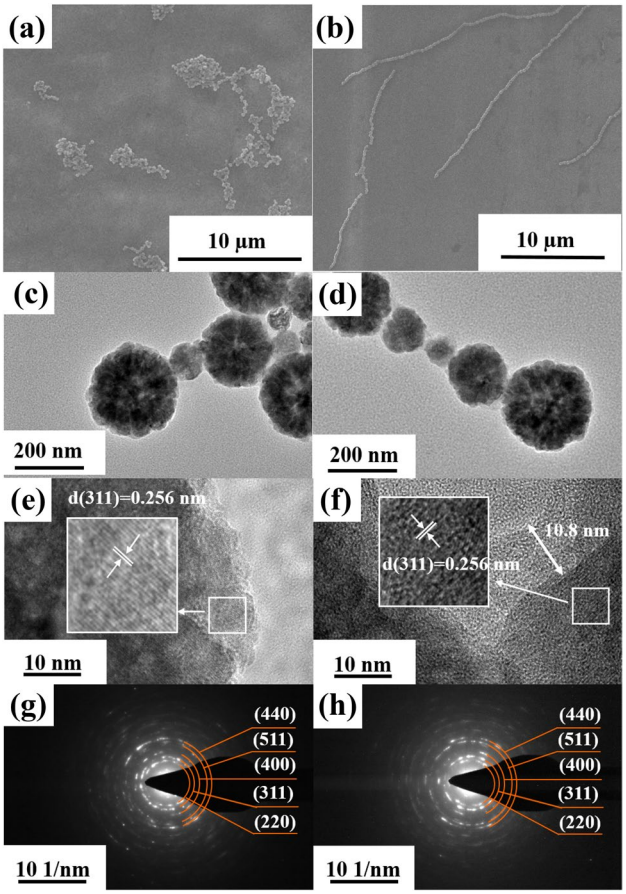

Fig. 1 SEM images of **a** pristine Fe_3O_4 nanoparticles and **b** chitosan-modified Fe_3O_4 nanochains; TEM images of **c** pristine Fe_3O_4 nanoparticles and **d** chitosan-modified Fe_3O_4 nanochains; HRTEM images of **e** pristine Fe_3O_4 nanoparticles and **f** chitosan modified Fe_3O_4 nanochains; selected area electron diffraction patterns of **g** pristine Fe_3O_4 nanoparticles and **h** chitosan-modified Fe_3O_4 nanochains

The magnetic properties of the pristine Fe_3O_4 nanoparticles and the chitosan-modified Fe_3O_4 nanoparticles are studied by VSM, and the hysteresis loops are given in Fig. 3. The coercivity *Hc* and saturation magnetization *Ms* for the chitosan-modified Fe_3O_4 nanoparticles are 49 Oe and 68 emu/g, respectively, which are lower than those for pristine Fe_3O_4 nanoparticles (*Hc* = 58 Oe, *Ms* = 152 emu/g). The decrease of *Ms* mainly attributes to the addition of nonmagnetic chitosan, which reduces the magnetic moments per unit mass.

To investigate the influence of chitosan content on the aggregation states of Fe_3O_4 nanoparticles, Fe_3O_4 nanoparticles with three different chitosan contents are prepared. Figure 4a shows that Fe_3O_4-1 aggregate together randomly due to their strong magnetic interactions. Figure 4b shows that Fe_3O_4-2 tend to form nanochains due to the decreased magnetic interactions. However, when the chitosan content was increased to 75 mg (Fig. 4c), the magnetic field intensity of each Fe_3O_4-3 nanoparticle is too weak to attract the nanoparticles nearby; therefore, most of the Fe_3O_4-3 nanoparticles are separated.

In order to investigate the chitosan contents in the Fe_3O_4-1, Fe_3O_4-2, and Fe_3O_4-3, FTIR and TGA have been carried out. It is found in Fig. 5a that FTIR spectra reveal several characteristic absorption peaks of Fe_3O_4 and chitosan. The peak observed at 563 cm^{-1} is assigned to Fe–O vibration of Fe_3O_4 component (Rahmanzadeh et al. 2014). For the chitosan component, the peaks at 2835 and 1375 cm^{-1} correspond to C–H stretching vibrations, while another peak at 1252 cm^{-1} is assigned to C–N vibration (Le VT et al. 2018). As shown in the Fig. 5a, the peak at 563 cm^{-1} for Fe_3O_4-1 is stronger than those for Fe_3O_4-2 and Fe_3O_4-3, indicating that Fe_3O_4-1 has the highest Fe_3O_4 content. It is also found that the peak at 1252 cm^{-1} for

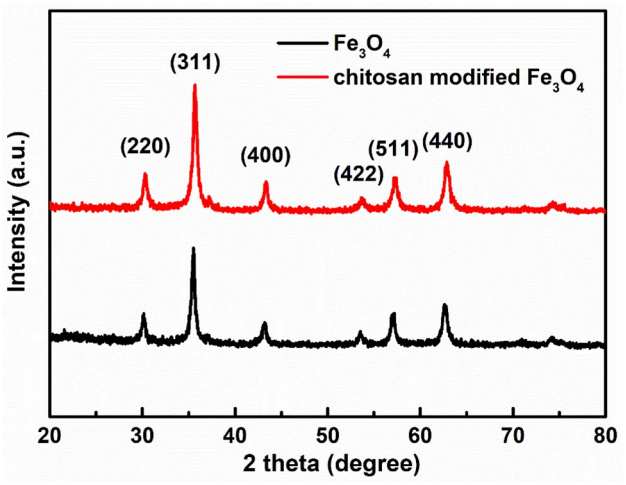

Fig. 2 XRD patterns of the pristine Fe_3O_4 nanoparticles and the chitosan-modified Fe_3O_4 nanoparticles

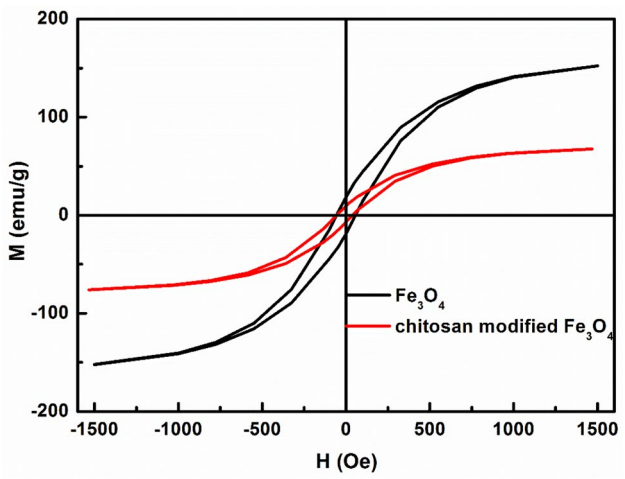

Fig. 3 Hysteresis loops of the pristine Fe_3O_4 nanoparticles and chitosan-modified Fe_3O_4 nanoparticles

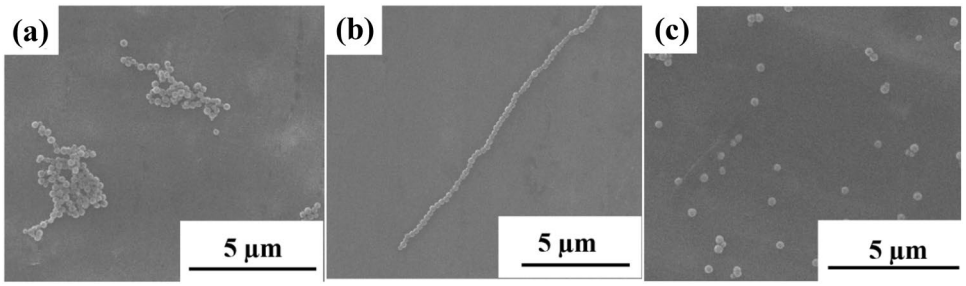

Fig. 4 SEM images of Fe_3O_4 nanoparticles: **a** Fe_3O_4-1, **b** Fe_3O_4-2, and **c** Fe_3O_4-3

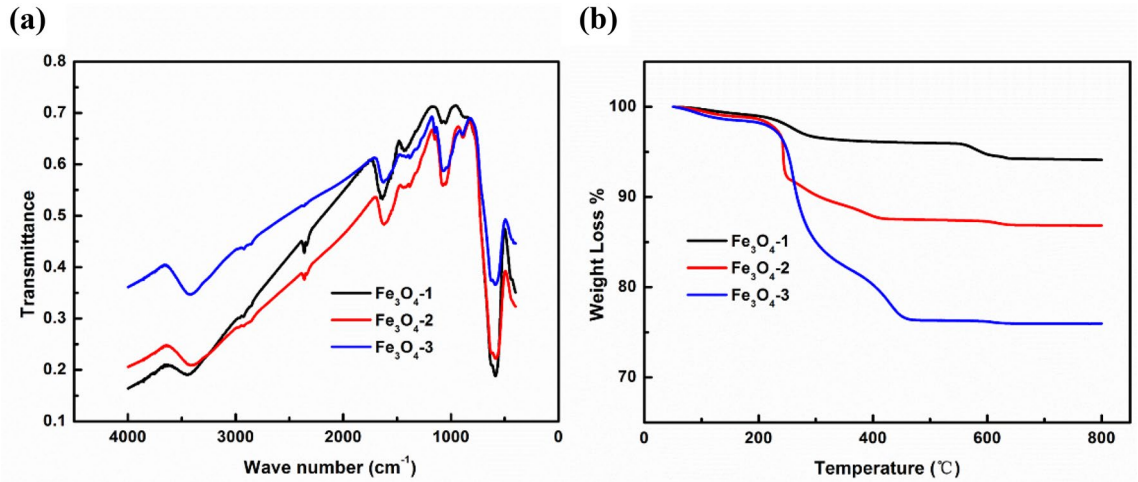

Fig. 5 **a** FTIR spectra of Fe_3O_4-1, Fe_3O_4-2, and Fe_3O_4-3. **b** TGA curves of the Fe_3O_4-1, Fe_3O_4-2 and Fe_3O_4-3

Fe_3O_4-3 is stronger than those for Fe_3O_4-1 and Fe_3O_4-2, showing that Fe_3O_4-3 has the highest chitosan content.

Figure 5b shows the TGA curves from room temperature up to 800 °C in air. In the range of 220–420 °C, the weight losses of Fe_3O_4-2 and Fe_3O_4-3 are about 13.15% and 24.04%, respectively, corresponding to the release of physically adsorbed water and thermal decomposition of the chitosan. For the Fe_3O_4-1 sample without chitosan modification, only 5.87% weight loss only due to the adsorbed water is observed. Supposing that the absorbed water are almost the same in the three samples, the chitosan contents in Fe_3O_4-2 and Fe_3O_4-3 are estimated to be approximately 7% and 18%, respectively.

To further verify the experiments, the magnetic field distributions of a single Fe_3O_4 nanoparticle with different thicknesses of chitosan are simulated by COMSOL (Comsol Multiphysics software), where the size of Fe_3O_4 nanoparticles is set to be 200 nm and the thicknesses of chitosan are set to be 0, 10 and 40 nm. Moreover, since the Fe_3O_4 nanoparticles have been magnetized by a magnetic stirring apparatus during the synthesis and modification process; therefore, the magnetic property of each Fe_3O_4 nanoparticle is anisotropic. In the simulation, two sides of each nanoparticle were set as two magnetic poles. The magnetic field distributions of the Fe_3O_4 nanoparticles with chitosan layers of 0 nm, 10 nm and 40 nm are shown in Figs. 6a–c, respectively, and the variation of magnetic field intensities at the top and side of each nanoparticle against chitosan thickness is plotted in Fig. 6d. The magnetic field intensity at the top of the single Fe_3O_4 nanoparticle without chitosan modification (Fig. 6a, d) is about 8.26×10^{-4} T, which is similar to both sides of the nanoparticles (7.74×10^{-4} T). Hence, the single Fe_3O_4 nanoparticle has almost the same strong magnetic attractions in different directions. This is the reason for the aggregation of the Fe_3O_4 nanoparticles.

As the thickness of chitosan increases, both top and side magnetic field intensities of Fe_3O_4 nanoparticles decrease. When the thickness of chitosan is 10 nm (Fig. 6b, d), the difference of magnetic field intensities between the top and side of nanoparticles is maximum. The magnetic field intensity at the top part is 3.04×10^{-4} T, which is much weaker than the both sides of the nanoparticles (6.17×10^{-4} T). Therefore, the other nanoparticles nearby would be attracted by the left or right side of the Fe_3O_4 nanoparticles, leading to the formation of nanochains.

When the thickness of chitosan is increased to 40 nm (Fig. 6c, d), however, there is a little difference in magnetic field intensities between the top and side of the particle.

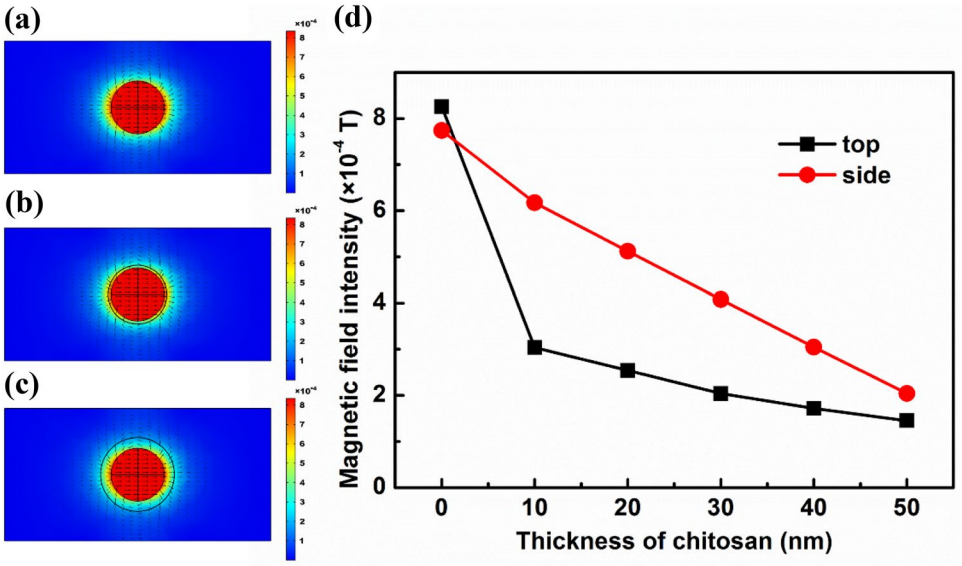

Fig. 6 Magnetic field distributions of Fe_3O_4 nanoparticles with different thicknesses of chitosan layers of **a** 0 nm, **b** 10 nm and **c** 40 nm, **d** Magnetic field intensities at the top and the side of Fe_3O_4 nanoparticles against the thickness of chitosan

The magnetic field intensity at the top part of particle is decreased to 1.72×10^{-4} T, and that at the both sides also decreased to 3.05×10^{-4} T. Therefore, the magnetic attractions for Fe_3O_4 nanoparticles with chitosan thickness of 40 nm are very weak even at the both sides of the particles, which is not strong enough to attract other nanoparticles nearby, leading to the distribution of separated nanoparticles. The theoretical simulations agree well with the experiment results.

The magnetic field distributions of nanochains are also simulated by COMSOL, where the size of Fe_3O_4 nanoparticles is set to be 200 nm and the chitosan thickness is 10 nm. In Fig. 7a, three Fe_3O_4 nanoparticles attract each other due to the strong magnetic interactions between magnetic poles. The magnetic field intensity around the middle part of the three particles is about 8.87×10^{-4} T, which is slightly stronger than those at two ends of the Fe_3O_4 nanochain (7.15×10^{-4} T). Figure 7d shows when another particle comes to join the group of three particles, there are two possible positions for it to connect: the ends or the middle part of the three Fe_3O_4 nanoparticles. As there are two contact points at the middle part, the newcomer would be more likely attached in the middle than at

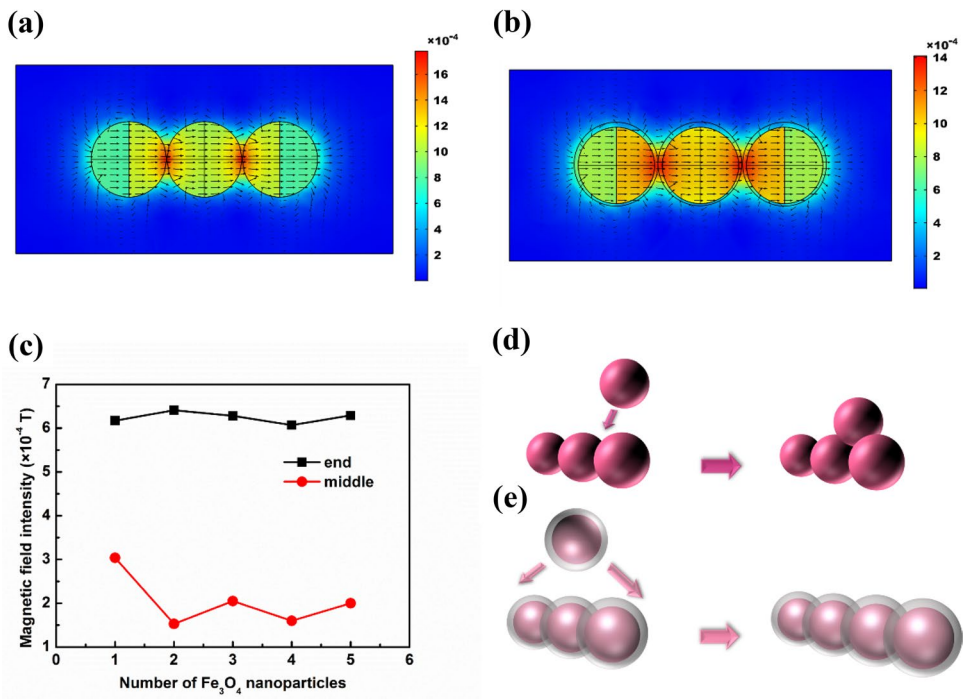

Fig. 7 The formation mechanism of Fe_3O_4 nanochains: **a** Magnetic field distribution of a nanochain formed by three pristine Fe_3O_4 nanoparticles, **b** Magnetic field distribution of a nanochain formed by three chitosan-modified Fe_3O_4 nanoparticles, and **c** Magnetic field intensities at the end and middle parts of the Fe_3O_4 nanochains with different number of nanoparticles in the chain, and each Fe_3O_4 nanoparticle has a chitosan layer of 10 nm, **d** Schematic of the aggregated Fe_3O_4 nanoparticles, and **e** Schematic of self-assembled chitosan-modified Fe_3O_4 nanochains

the ends because this is more stable and energetically favorable. Therefore, the nanochains would not be formed.

Figure 7b shows the magnetic field distribution of nanochain formed by three chitosan modified Fe_3O_4 nanoparticles with 10 nm chitosan layer, and Fig. 7c shows the magnetic field intensities at the end and middle parts of the nanochain against the nanoparticles number in the chain. All Fe_3O_4 nanoparticles in Figs. 7b, c have a chitosan layer of 10 nm. For the chitosan-modified nanoparticles, the magnetic field intensity around the middle part of the three nanoparticles is about 2.05×10^{-4} T, much lower than those at two ends of the nanochain (6.28×10^{-4} T). Moreover, as shown in Fig. 7c, although the number of Fe_3O_4 nanoparticle increases, the magnetic field intensities at the end and middle parts of Fe_3O_4 nanochain do not change a lot, and the magnetic field intensity in middle part is much weaker than the ends of the Fe_3O_4 nanochain. As shown in Fig. 7e, when another nanoparticle comes, the two ends of the nanochain are the preferential positions to attract it due to the stronger field intensities, leading to the formation of a longer nanochain. These simulation results are consistent with the experimental results.

Conclusions

The self-assembled Fe_3O_4 nanochains have been prepared by controlling the chitosan thickness coated on the surface of Fe_3O_4 nanoparticles. Both numerical simulations and experiments demonstrated that the magnetic field intensities at top and side of a single Fe_3O_4 nanoparticle decrease with increasing chitosan thickness. As the chitosan thickness changes from 0 to 10 nm and 40 nm, the state of Fe_3O_4 nanoparticles goes from aggregation to nanochains and separated ones. Furthermore, when the chitosan thickness is 10 nm, the difference of magnetic field intensities between the top and side of a single Fe_3O_4 nanoparticle reaches the maximum, and remains stable although the number of Fe_3O_4 nanoparticle is increased. Therefore, coating with 10 nm chitosan layer is the optimum condition for the formation of Fe_3O_4 nanochains. The chitosan-modified Fe_3O_4 nanochains may have potential applications in biomedical area, including but not limited to artificial skin, artificial cartilage, tendon and clinical cancer treatment.

Acknowledgements This work was supported by the National Natural Science Foundation of China (No. 51972039,51661145025) and Liaoning Revitalization Talents Program (No. XLYC1902122).

Compliance with ethical standards

Conflict of interest The authors declare that they have no financial and personal relationships with other people or organizations that can influence our work.

References

Berrod Q, Lyonnard S, Guillermo A, Ollivier J, Frick B, Manseri A, Ameduri B, Gebel G (2015) Nanostructure and transport properties of proton conducting self-assembled perfluorinated surfactants: a bottom-up approach toward PFSA fuel cell membranes. Macromolecules 48:6166–6176

Gao D, Guo X, Zhang X, Chen S, Wang Y, Chen T, Huang G, Gao Y, Tian Z, Yang Z (2020) Multifunctional phototheranostic nanomedicine for cancer imaging and treatment. Mater Today Bio 5:100035

Gong J, Li S, Zhang D, Zhang X, Liu C, Tong Z (2010) High quality self-assembly magnetite (Fe_3O_4) chain-like core-shell nanowires with luminescence synthesized by a facile one-pot hydrothermal process. Chem Commun 46:3514–3516

Gortari MC, Hours RA (2013) Biotechnological processes for chitin recovery out of crustacean waste: a mini-review. Electron J Biotechn 16:14

Kandra P, Challa MM, Jyothi HKP (2012) Efficient use of shrimp waste: present and future trends. Appl Microbiol Biotechnol 93:17–29

Kim Y, Choi YS, Lee HJ, Yoon H, Kim YK, Oh M (2014) Self-assembly of fluorescent and magnetic Fe_3O_4@coordination polymer nanochains. Chem Commun 50:7617–7620

Le VT, Doan VD, Nguyen DD, Nguyen HT, Ngo QP, Tran TKN, Le HS (2018) A novel cross-linked magnetic hydroxyapatite/chitosan composite: preparation, characterization, and application for Ni(II) ion removal from aqueous solution. Water Air Soil Pollut 229:101

Li X, Niu XD, Li Y, Chen MF (2018) Self-assembly of silica microparticles in magnetic multiphase flows: experiment and simulation. Phys Fluids 30:040905

Lin B, Li Q, Liu B, Zhang S, Chao D (2016) Biochemistry-directed hollow porous microspheres: bottom-up self-assembled polyanion-based cathodes for sodium ion batteries. Nanoscale 8:8178–8188

Lvov YM, Pattekari P, Zhang X, Torchilin V (2011) Converting poorly soluble materials into stable aqueous nanocolloids. Langmuir 27:1212–1217

Oster J, Parker J, Brassard LA (2001) Polyvinyl-alcohol-based magnetic beads for rapid and efficient separation of specific or unspecific nucleic acid sequences. J Magn Magn Mater 225:145–150

Parekh G, Shi Y, Zheng J, Zhang X, Leporatti S (2018) Nano-carriers for targeted delivery and biomedical imaging enhancement. Ther Deliv 9:451–468

Rahmanzadeh L, Ghorbani M, Jahanshahi M (2014) Synthesis and characterization of Fe3O4@polyrhodanine nanocomposite with core–shell morphology. Adv Polym Technol 33:21463

Schotte L, Rombaut B, Thys B (2012) A liquid phase affinity capture assay using magnetic beads to study protein-protein interaction: the poliovirus-nanobody example. Jove-J Vis Exp 63:3937

Seifan M, Ebrahiminezhad A, Ghasemi Y, Samani AK, Berenjian A (2018) Amine-modified magnetic iron oxide nanoparticle as a promising carrier for application in bio self-healing concrete. Appl Microbiol Biot 102:175–184

Silva RTD, Mantilaka MMMGPG, Ratnayake SP, Amaratunga GAJ, Silva KMND (2017) Nano-MgO reinforced chitosan nanocomposites for high performance packaging applications with improved mechanical, thermal and barrier properties. Carbohyd Polym 157:739–747

Song J, Wu B, Zhou Z, Zhu G, Chen X (2017) Double-layered plasmonic-magnetic vesicles by self-assembly of janus amphiphilic Au-Fe_3O_4 nanoparticles. Angew Chem Int Ed 56:8110–8114

Sun L, Sun J, Chen L, Niu P, Yang X, Guo Y (2017) Preparation and characterization of chitosan film incorporated with thinned

young apple polyphenols as an active packaging material. Carbohyd Polym 163:81–91
Vergaro V, Scarlino F, Bellomo C, Rinaldi R, Vergara D, Maffia M, Baldassarre F, Giannelli G, Zhang X, Lvov YM, Leporatti S (2011) Drug-loaded polyelectrolyte microcapsules for sustained targeting of cancer cells. Adv Drug Deliv Rev 63:847–864
Verlee A, Mincke S, Stevens CV (2017) Recent developments in antibacterial and antifungal chitosan and its derivatives. Carbohyd Polym 164:268–283
Wan J, Cai W, Meng X, Liu E (2007) Monodisperse water-soluble magnetite nanoparticles prepared by polyol process for high-performance magnetic resonance imaging. Chem Commun 47:5004–5006
Wang J, Kawde AN, Erdem A, Salazar M (2001) Magnetic bead-based label-free electrochemical detection of DNA hybridization. The Analyst 126:2020–2024
Wang SH, Shi XY, Antwerp MV, Cao ZY, Swanson SD, Bi XD, Baker JR Jr (2007) Dendrimer-functionalized iron oxide nanoparticles for specific targeting and imaging of cancer cells. Adv Funct Mater 17:3043–3050
Zhang JH, Du J, Ma DK, Xi G, Hu XB, Qian YT (2007) One-dimensional chain Fe_3O_4 nanoparticles encapsulated in worm-shaped carbon shell. Solid State Commun 144:168–173
Zhang Y, Sun L, Fu Y, Huang ZC, Zhai HR (2009) The shape anisotropy in the magnetic field-assisted self-assembly chain-like structure of magnetite. J Phys Chem C 113:8152–8157
Zou W, Chen Y, Zhang X, Li J, Sun L, Gui Z, Du B, Chen S (2018) Cytocompatible chitosan based multi-network hydrogels with antimicrobial, cell anti-adhesive and mechanical properties. Carbohyd Polym 202:246–257

Publisher's Note Springer Nature remains neutral with regard to jurisdictional claims in published maps and institutional affiliations.